Nanoscale

Effects of thermally-induced changes of Cu grains on domain structure and electrical performance of CVD-grown graphene

Yaping Wu,[a,b] Yufeng Hao,*[b,c] Mingming Fu,[a] Wei Jiang,[a] Qingzhi Wu,[b] Peter A. Thrower,[d] Richard D. Piner,[b] Congming Ke,[a] Zhiming Wu,[a] Junyong Kang*[a] and Rodney S. Ruoff*[b,e]

During the chemical vapor deposition (CVD) growth of graphene on Cu foils, evaporation of Cu and changes in the dimensions of Cu grains in directions both parallel and perpendicular to the foils are induced by thermal effects. Such changes in the Cu foil could subsequently change the shape and distribution of individual graphene domains grown on the foil surface, and thus influence the domain structure and electrical properties of the resulting graphene films. Here, a slower cooling rate is used after the CVD process, and the graphene films are found to have an improved electrical performance, which is considered to be associated with the Cu surface evaporation and grain structure changes in the Cu substrate.

Introduction

Graphene has attracted recent interest due to its distinctive band structure and physical properties.[1–10] Among various methods, such as micromechanical cleavage,[1] growth on metal substrates,[11–13] thermal decomposition of SiC,[14,15] and graphene oxide reduction,[16,17] the chemical vapor deposition (CVD) of hydrocarbon precursors on metal substrates is widely used to achieve large-area and high-quality graphene films.[11,18] Various transition metals, including ruthenium (Ru),[19] iridium (Ir),[20] nickel (Ni),[13] copper (Cu),[11] and several binary alloys[21,22] including Ni–Mo and Cu–Ni, have been used as substrates for the CVD growth of graphene. Graphene films grown on Ru usually have layers with a non-uniform thickness, and bonding between the bottom layer and the Ru surface can affect their properties.[19] On the other hand, graphene grown on Ir is weakly bonded such that the growth is less dependent on substrate conditions, and the layers can be highly ordered while slightly rippled; such rippling is stated to lead to mini-gaps in the electronic band-structure.[20] Polycrystalline Ni foils typically have grain sizes of tens of microns, and yield graphene films with a relatively small grain size and variable thickness.[13] Cu and Ni–Mo alloy have been reported as excellent substrates for generating monolayer graphene, and a single-crystal domain size can be as large as a centimeter.[18] Here, we focus on low-cost Cu foils as the substrate because they have been the substrate of choice for the scaled growth of graphene films.[23] In our previous work, changes in the Cu grains during graphene growth were found to influence the local atomic arrangement in the dendritic-shaped graphene domains.[24] Here, the effects on the domain structure and electrical performance of the graphene films are further studied.

Partial- and full-coverage graphene films were grown by CVD from methane and hydrogen on polycrystalline Cu foils. Electron back-scatter diffraction (EBSD), optical and atomic force microscopy (AFM) were used to identify Cu grain boundaries (GBs) and the orientations of Cu grains before and after thermal annealing so that the changes in the grain structure of the Cu foils can be observed. Scanning electron microscopy (SEM) was used to observe the partial coverage graphene on Cu substrate, with the results suggesting that the changes of both the shape and location of individual graphene domains were affected by the thermal evolution of Cu grains. As the individual domains grow and merge to yield a complete film, such evolution of the Cu grains would influence the graphene grain structure and thus its electrical performance. As a result

[a]Fujian Provincial Key Laboratory of Semiconductors and Applications, Collaborative Innovation Center for Optoelectronic Semiconductors and Efficient Devices, Department of Physics, Xiamen University, Xiamen 361005, P. R. China. E-mail: jykang@xmu.edu.cn
[b]Department of Mechanical Engineering and the Materials Science and Engineering Program, The University of Texas at Austin, Austin, Texas 78712, USA. E-mail: yh2682@columbia.edu, ruofflab@gmail.com
[c]Department of Mechanical Engineering, Columbia University, New York, New York 10027, USA
[d]Department of Materials Science and Engineering, the Pennsylvania State University, University Park, PA 16802, USA
*[e]Center for Multidimensional Carbon Materials and Department of Chemistry and School of Materials Science Ulsan National Institute of Science and Technology (UNIST), Ulsan, 689-798, South Korea*

of these studies, improved growth conditions were formulated that led to the production of graphene with a higher electronic conductivity.

Results and discussion

For low-pressure CVD from methane and hydrogen on Cu foils, graphene grows through a surface-mediated mechanism,[25] and thermally-induced changes in the Cu grains at high temperature may influence the atomic arrangement in the grown graphene.[24] Therefore, prior to investigating the effects of annealing on the properties of a CVD graphene film on a Cu foil, changes in the Cu grain structure were studied. Fig. 1(a) displays the EBSD map of an as-received Cu foil before graphene growth. The polycrystalline Cu foil was found to have grains of different shapes and orientations whose sizes were mostly between 5–20 μm. After graphene growth (Experimental section), the Cu grains have grown to the millimeter scale, as shown in the EBSD map in Fig. 1(b), consistent with previous reports.[26,27] To study the subsequent thermal effect on Cu grains, a 10 min annealing at 1000 °C was performed for the graphene–Cu sample (Experimental section) after the orientation measurement in Fig. 1(b). The EBSD map for the same area is shown in Fig. 1(c). Comparing the Cu crystallographic orientations (distinguished by different colors) of the as-grown sample and that after further annealing, the average grain sizes remain similar, but the crystal orientations of the grains are obviously changed.

Fig. 2 shows photographs of the front and back surfaces of one Cu foil after graphene growth [2(a) and (b)], and after further annealing [2(c) and (d)]. It can be seen that grains with different orientations have different brightness so that the sizes and shapes of the Cu grains are easily determined. After graphene growth, most of the Cu grains have irregular shapes, with sizes ranging from hundreds of microns to the centimeter scale. Based on a comparison of the images in Fig. 2(a) and (b), the Cu grains on the front and back surfaces of the foil are
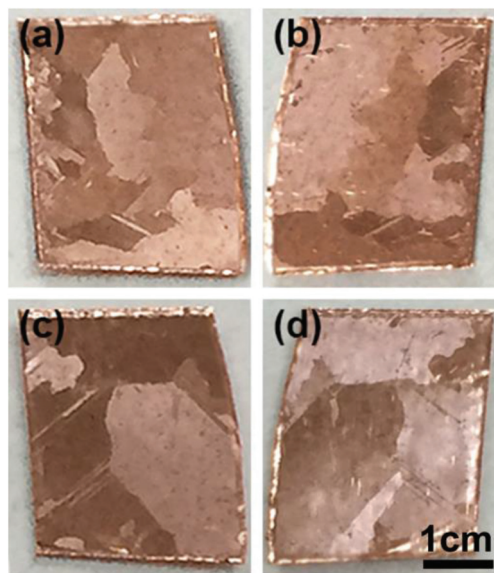
Fig. 2 (a) and (b) Photographs of the front and back surfaces of a Cu foil that were acquired after graphene growth; (c) and (d) front and back surfaces of the Cu foil after further annealing (Experimental section).

almost mirror images of each other. That is, if one chooses a small area on one side of the foil, it will contain only one grain in the 'through foil' direction. The GBs completely penetrate the foil and have essentially the same spatial distribution on each side of the foil. After further annealing, the grain structure, including size and shape, was found to have changed, as shown in Fig. 2(c). By comparing Fig. 2(c) and (d), the morphologies of the grains on the front and back surfaces are changed simultaneously and still mirror images of each other. This suggests that the further annealing not only causes surface evaporation of Cu but also changes the grain shape and orientation in directions both parallel and perpendicular to the foil.
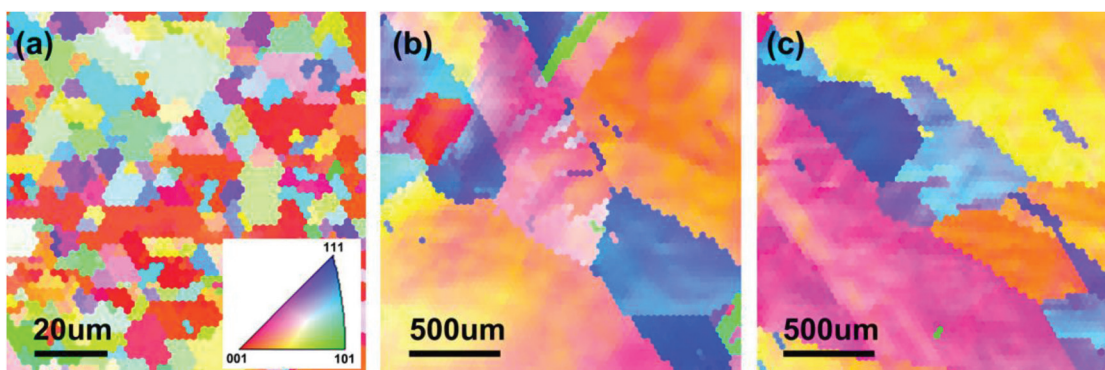

Fig. 1 (a)–(c) EBSD orientation maps on a Cu foil: (a) original Cu foil; (b) after the growth of partial-coverage graphene and cooling to room temperature (RT) with a cooling rate of 0.5 °C s^{-1}; (c) the same area with (b) that after further annealing at 1000 °C for 10 min and cooling to RT with a cooling rate of 0.5 °C s^{-1} (Experimental section).

Optical microscopy was used to study the Cu GBs, as shown in Fig. 3(a) and (b), which are images of the same area on the front and back surfaces of the Cu foil, respectively. The blue arrows denote a GB appearing as a "black curve" on both surfaces with a similar shape, which suggests that the GB penetrates the foil and divides adjacent grains. Differently, the red arrows indicate GBs that appear as demarcation lines between two adjacent grains with obvious contrast difference. In contrast to the GBs that go from the top to the bottom surface of the Cu foil, such demarcation lines are separately distributed on each surface, because the grain structures of the two symmetrical surfaces are different from each other. For comparison, the red dashed lines in Fig. 3(d) show the GBs on the Cu surface in Fig. 3(c). The adjacent two grains with such GB are usually less thick (see the AFM images below), and do not penetrate the Cu foil. The surface morphologies of these different GBs (penetrating and terminating inside the Cu foil, respectively) were further investigated by AFM, as shown in Fig. 3(e) and (f), which are respectively captured from the two blue dashed squares in Fig. 3(a); numbers 1, 2, and 3 mark the three GBs shown in the images. The adjacent Cu grains on either side of these GBs have different surface morphologies and roughness levels; the height profiles across the GBs are shown in Fig. 3(g). The height difference measured between the adjacent grains across GB 1 is about 320 nm, but is only

50 nm across GB 2 and is negligible across GB 3. This suggests that if the grains penetrate the Cu foil, their boundaries are more obvious and usually have a higher step, while if the grains terminate inside the foil, their steps are usually much smaller or even hard to distinguish. Such two kinds of GBs are thus typically present for a Cu foil, and both can be changed because of the evolution of Cu grains by heat treatment.

Such drastic changes in the structure of the Cu grains could influence the morphology of the grown graphene domains. Fig. 4(a)–(f) show SEM images of dendritic-shaped graphene domains on the Cu before and after annealing, respectively. In Fig. 4(a), a 'deep' Cu GB denoted by the blue arrow is obvious before annealing, which indicates that the graphene domains in the image span two adjacent Cu grains, while the domains in Fig. 4(b) are located within one single Cu grain, because no Cu GB is observed over this area. The as-grown graphene domains have a lateral dimension of less than 50 μm, and the distances between the domains are measured to yield the relative positions of these domains, as indicated by the yellow arrows. After 10 min annealing at 1000 °C (Experimental section), the original Cu GB disappears completely, but some new boundaries and many steps on the Cu appear instead, as shown in Fig. 4(d) and (e). Because of such changes in the grain structure of the Cu substrate, graphene domains move, with the distance between domains decreasing [Fig. 4(d)] or increasing [Fig. 4(e)] depending on contraction or expansion of the local Cu grains. In addition to the changing spatial distribution of the graphene domains, individual domains are influenced by the evolving grain structure, as shown in Fig. 4(c) and (f). The lateral scale along the diagonals of the four lobes remains the same, whereas the angles between adjacent lobes are obviously changed after annealing. For example, the angle between the two nearest lobes decreases from 55° to 46°, which shows that the evolution of the Cu grain structure can also affect the shape of the individual graphene domains. As a control experiment to test the instrument response function of the SEM, the graphene–Cu sample was repeatedly loaded and imaged in the same region before annealing and it was found that the shape and distribution of the graphene domains remained unchanged without annealing.

EBSD maps of the graphene–Cu samples were obtained from the same area before and after annealing to determine the crystal orientations of the underlying Cu grains, as shown in Fig. 5. The corresponding SEM images are displayed to compare the morphology of the grown graphene domains. This area contains three Cu grains before annealing, with GBs readily identified in the SEM image shown in Fig. 5(a). The EBSD characterization in Fig. 5(b) shows that the three grains have two different orientations, with Cu (103) and Cu (547) planes (represented by yellow and purple, respectively) parallel to the surface. Some graphene domains span neighboring Cu grains. After annealing, the Cu grains drastically change in terms of both size and orientation. As shown in Fig. 5(c), two new GBs are generated, accompanied by the disappearance of the original GBs in Fig. 5(a). The two new GBs divide the Cu surface into three grains, whose crystal planes are close to the
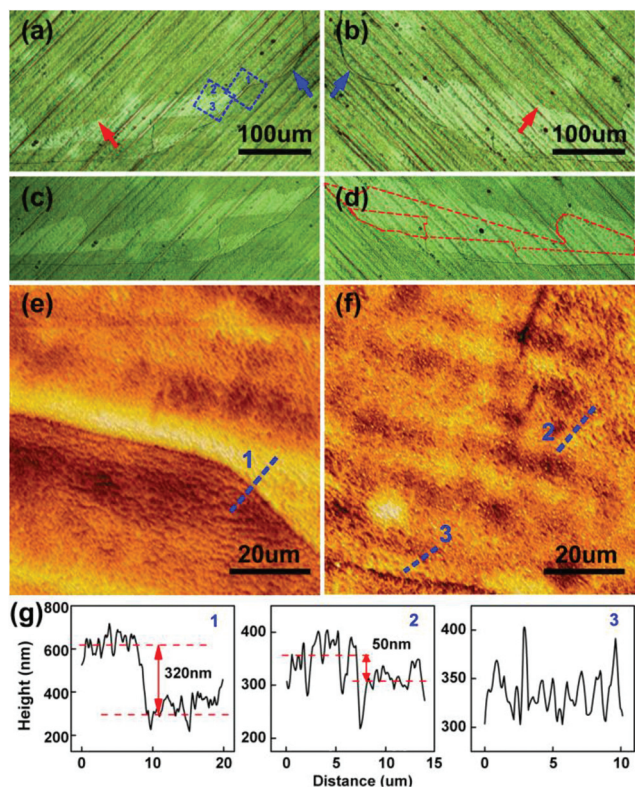
Fig. 3 (a)–(d) Optical images of the front and back surfaces of a Cu foil; (e) and (f) AFM images taken from the two blue dashed square regions in (a); (g) height profiles measured across the GBs 1, 2, and 3 in (e) and (f).
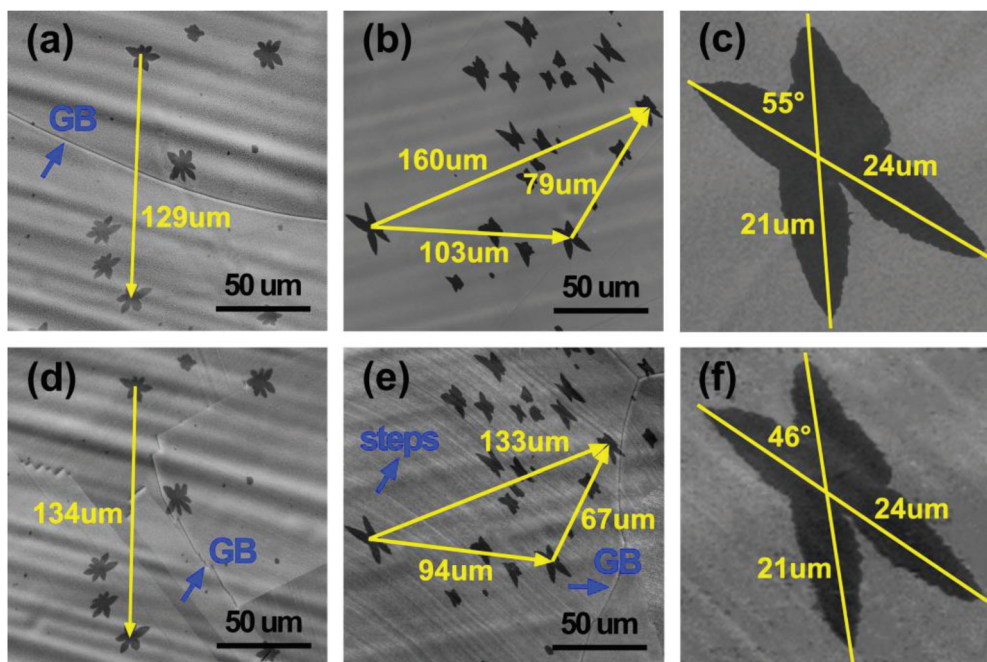
Fig. 4 (a)–(c) SEM images of the as-grown dendritic-shape graphene domains on Cu foil; (d)–(f) the same regions as in (a)–(c) but acquired after a 10 min annealing at 1000 °C (Experimental section). The blue arrows indicate the Cu GBs and steps that emerge and disappear after the annealing. The yellow arrows denote the relative distances of the graphene domains that are changed after the annealing process.
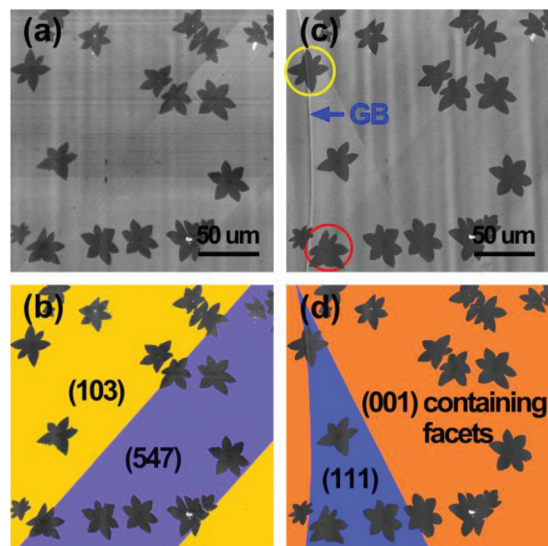

Fig. 5 SEM and the corresponding EBSD orientation maps of the graphene–Cu sample before and after annealing: (a) and (c) as-grown graphene domains on Cu foil; (b) and (d) after a 10 min annealing at 1000 °C and cooling to RT (Experimental section). The red circle in panel (c) indicates a 6-lobed graphene domain, below which a Cu GB disappears after the annealing, while the yellow circle indicates another graphene domain, below which a Cu GB (denoted by the blue arrow) forms after the annealing.

Cu (001) or Cu (111), denoted by orange and blue in Fig. 5(d), respectively. According to the face-centered cubic (fcc)-structure for Cu, the lattice planes and atomic configurations for the grain orientations mentioned above are schematically shown in Fig. 6. To examine the atomic arrangements, the Cu atoms in the fcc unit cell are projected on these 2D lattice planes. Accordingly, the rotation angles of the lattice planes before and after annealing are calculated to be about 18.5° and 43.1° for Cu (103) to Cu (001), and to Cu (111), respectively; and 42.5° and 13.2° from Cu (547) to Cu (001), and to Cu (111), respectively. The average packing densities change from 0.497 [Cu (103)] and 0.166 [Cu (547)] to 0.785 [Cu (001)] and 0.907 [Cu (111)]. The red and yellow circles in Fig. 5(c) highlight typical graphene domains, beneath which the original neighboring Cu grains merge into a single grain or in which one grain splits into two grains with different crystal orientations. In both cases, no observable mechanical damage is introduced to the graphene domains during the high-temperature annealing. This suggests that although the shapes of the individual domains are deformed by the movement of the Cu substrate, the morphology of the domains remains more or less the same even along the Cu GBs. Hence, we speculate that Cu GBs normally present underneath the graphene can be formed not only before graphene growth but also afterwards in the subsequent high-temperature environment. During the evolution of the grain structure of the Cu substrate, deformation of the graphene domains is more likely through the distortion of C–C bonds[24] and the formation of small wrinkles and graphene GBs rather than by tearing the graphene within the domains.

The above experimental results demonstrate the effects of the evolution of Cu grains on the shape and distribution of the graphene domains that partially cover them. As the individual
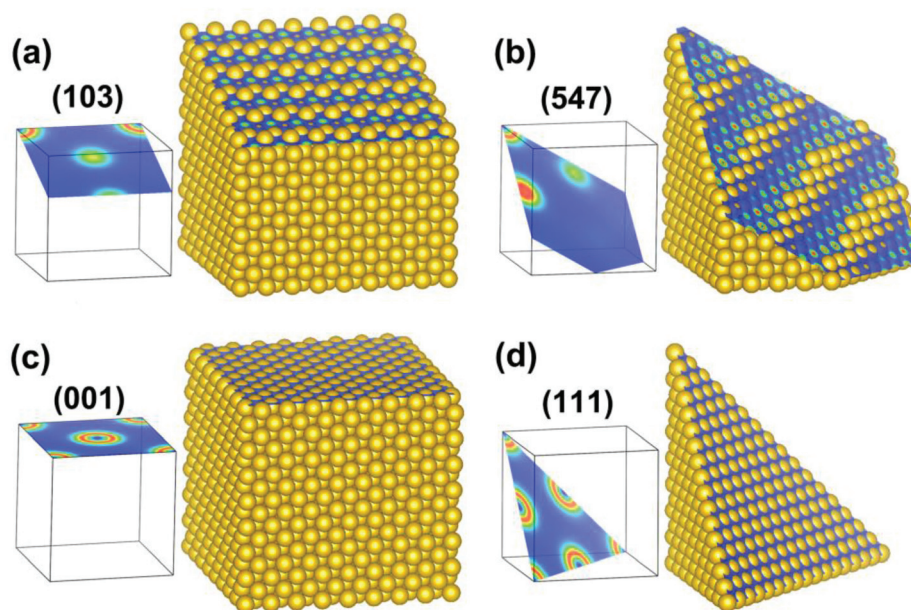
Fig. 6 Diagrams of Cu lattice planes and atomic configurations of (a) Cu (103), (b) Cu (547) before annealing, and (c) Cu (001), (d) Cu (111) after annealing. The left transparent cubes display 2D projections of Cu atoms on these lattice planes in the fcc unit cell.

domains grow and merge into a film, the movement of graphene domains will induce an accumulation of tensile and compressive stresses within the growing graphene film, which may lead to local deformation or the development of structural defects during the growth process, as mentioned in our previous work.[24] Therefore, the size of single-crystal graphene domains depends not only on the nucleation density but also on the subsequent growth process. As surface-mediated growth,[25] it is generally considered that the average size of graphene domains for a full-coverage film on a Cu foil is determined by the growth temperature, time, gas flow, pressure, and substrate conditions, but that it is independent of the cooling rate. However, we believe the cooling rate can be a factor associated with the evolution of the Cu substrate, and thus influences the GBs in the graphene film. To address this issue, three full-coverage graphene monolayers were prepared and named samples 1, 2, and 3. For these three samples, the growth conditions, including annealing under H_2 (2 sccm), methane flow rate (1 sccm) and partial pressure (16.5 mTorr), growth time (12 min) and temperature (1000 °C), were kept constant while using different cooling rates of 2.5, 0.5, and 0.08 °C s^{-1}, respectively. To probe the GBs in the graphene monolayers, a selective oxidizing method was performed in air at 180 °C for 2 h.[28,29] When in contact with air, the intact graphene is a layer that protects the underlying Cu film from oxidation and oxygen atoms have to diffuse to the Cu substrate through defects in the graphene film. Therefore, oxidation occurs only at the Cu surface below these defects. In this way, structural defects such as point defects and GBs are clearly emphasized, as shown in the SEM images in Fig. 7(a)–(c) for samples 1, 2, and 3, respectively. The gray areas are the graphene-covered Cu surfaces, which are decorated with a series

of white lines. The lateral dimension of the white lines is estimated to be about 500 nm to 1 μm, and the density decreases from samples 1 to 3. Fig. 7(d) shows a high-resolution SEM image of the graphene–Cu surface from sample 1 after the oxidation treatment. The thick irregular white lines are formed by a row of particles, and some isolated particles are also found at gaps in the lines. To determine the compositions of these particles, energy dispersive X-ray spectroscopy (EDS) spectra were captured at both the white line and the graphene areas, and are shown in Fig. 7(e). The spectra are dominated by peaks at energies of 0.94, 8.04, 8.90 keV, which are assigned to elemental Cu from the substrate. Additionally, there are two signal peaks at 0.28 and 0.52 keV, which originate from C and O, respectively. At the graphene areas, the C signal is obviously stronger than that of the O, whereas in the white lines, the O peak has the higher intensity. This suggests that the white lines have a much higher O content, which is attributed to the oxidized Cu surface where the graphene GBs exist. Accordingly, the density of the white lines reflects the scale of the single-crystal graphene domains. Therefore, the average size of the single-crystal domains increases from sample 1 to sample 3 and is inversely related to the cooling rate. Thus, the use of a slower cooling rate can be beneficial to relieve the accumulated stresses, which leads to a lower defect density and larger single-crystal domains in the monolayer graphene films.

The improvement of the graphene lattice quality is further reflected in the improved carrier mobility in FET measurements. For fabricating FET devices, the three graphene films were transferred onto SiO_2/Si (SiO_2 thickness: 285 nm) substrates. In order to evaluate their general electronic properties, a special large channel dimension of 1 mm × 5 mm was applied for the FET devices. Fig. 8(a) shows a typical optical
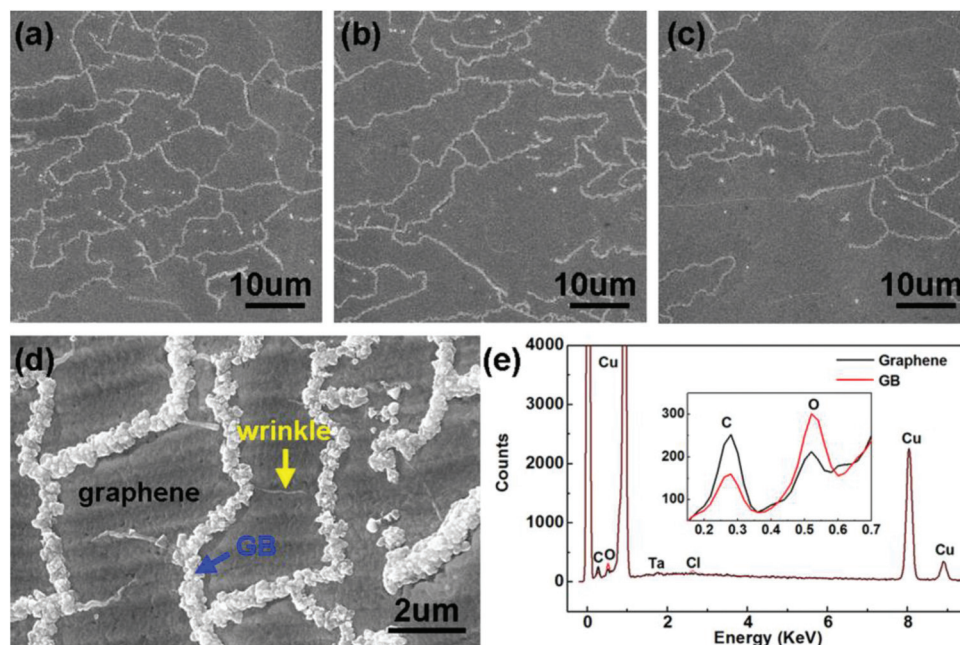
Fig. 7 (a)–(c) SEM images of the oxidized graphene–Cu samples obtained with average cooling rates of: (a) 2.5 °C s⁻¹, (b) 0.5 °C s⁻¹, and (c) 0.08 °C s⁻¹; (d) and (e) high-resolution SEM image and the EDS measurements of the oxidized graphene–Cu sample with a cooling rate of 2.5 °C s⁻¹; the black and red spectra are respectively acquired from the clean graphene surface and the oxidized GB.

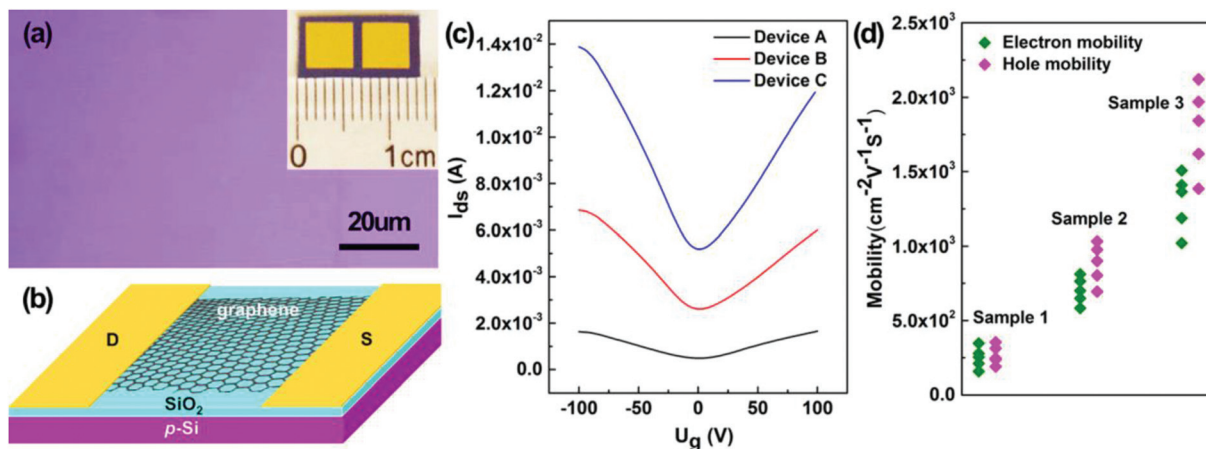**Fig. 8** (a) Optical microscopy image of a monolayer graphene film on a 285 nm–SiO$_2$/Si substrate, based on which the FET device was fabricated with a channel of 1 mm in length and 5 mm in width (inset); (b) schematic diagram of the graphene FET device used for electrical transport measurements; (c) the V_g dependent I_{ds} curves for devices A, B, and C, respectively; (d) statistic data of the carrier mobility measured from samples 1, 2, and 3.

image of the transferred graphene film, where the back-gate FET device was constructed, as shown by the photograph and diagram in Fig. 8(a) and (b), respectively. After degassing, the Dirac point is near the zero gate voltage, and the electron and hole conductions are symmetrical. The measured $I_{ds} - V_g$ curves for devices A, B, and C are shown in Fig. 8(c). The slopes reflect the carrier mobility (μ) according to the following equation:[30]

$$\mu = L/(WC_gV_{ds})(\Delta I_{ds}/\Delta V_g), \qquad (1)$$

where L and W are the channel length and width, respectively and C_g is the gate capacitance per unit area. Using this equation, the electron (hole) mobility can be calculated to be 254 (245), 700 (900), and 1410 (1970) cm^2 V^{-1} s^{-1} for devices A, B, and C, respectively. Obviously, the mobility of device C is about 5–8 times of that of device A, suggesting some relation to the cooling rate of the graphene grown on the Cu foil. To further verify the reliability of the experimental results, a series of electrical transport measurements were done for the three samples, and all the statistic data of the carrier mobility

exhibit a distinct increasing trend from sample 1 to sample 3, as shown in Fig. 8(d). Therefore, the use of a slower cooling rate produces a graphene film with a relatively higher carrier mobility, which improves the electrical performance.

Summary

Graphene films with partial and full coverage were grown on polycrystalline Cu foils by CVD. Optical microscopy and EBSD characterizations show that, in both the horizontal and vertical directions of the Cu foils, an entire movement of Cu grains as well as evaporation from the surface was induced by heat treatment. As a result, the sizes and orientations of the Cu grains were dramatically changed. Such changes in the Cu substrate led to changes in the individual graphene domains in terms of both shape and distribution. As the individual domains grew into a full-coverage monolayer, the movement of graphene portions resulted in tensile and compressive stresses within the film, and consequently led to local deformation and development of structural defects. A much slower cooling rate was found be beneficial in relieving the accumulated stresses, generating a graphene monolayer with a lower defect density and larger single-crystal domains. A corresponding improved electronic performance was verified by an apparent increase in carrier mobility in FET transport measurements.

Experimental section

Graphene growth and annealing of graphene–Cu[31]

Partial- and full-coverage graphene films were grown by CVD on 25 μm-thick 10 mm × 50 mm polycrystalline Cu foils. Before growth, a vacuum background of about 0.1 mTorr was achieved. The substrates were then heated to 1000 °C under 2 sccm H_2 (Air Gas Inc. 99.999%) and held at this temperature for 30 min to remove the surface oxide. 1 sccm CH_4 with a partial pressure of 16.5 mTorr was used as the gaseous carbon source. The growth temperature was 1000 °C, and the growth times were 1.5 and 12 min for partial- and full-coverage graphene films, respectively. The annealing of graphene–Cu was performed under 2 sccm H_2, by gradually increasing the temperature to 1000 °C and holding it at this temperature for 10 min. After this, the samples were cooled to RT with a cooling rate of 0.5 °C s^{-1}.

Oxidation treatment[28,29]

The oxidation of graphene–Cu samples was performed by a 2 h annealing in air at 180 °C.

Transfer of graphene[24,32]

As-grown partial- and full-coverage graphene films on Cu foils were spin-coated with a thin layer of poly methyl methacrylate (PMMA), and floated onto a $(NH4)_2S_2O_8$ aqueous solution (0.5 M) to etch the Cu substrate. After overnight exposure, suspended graphene/PMMA films floating on the solution were captured on SiO_2/Si (SiO_2 thickness: 285 nm) substrates (p^{++} doping, ρ = ~0.002–0.005 Ω cm) and dried in air. The final graphene films on SiO_2/Si substrates were obtained after immersing them in acetone for several hours to remove the PMMA.

SEM, EBSD and AFM characterization

SEM images were acquired using an FEI Quanta-600 FEG Environmental SEM with a beam voltage of 30 kV.[11] EBSD measurements were performed with a Zeiss Neon40 FE-SEM (EDAX Pegasus integrated EDS & EBSD system). The accelerating voltage of the primary electron beam was 15 kV, and the aperture diameter was 120 μm. The AFM images and height profiles were obtained with a SPA400 AFM system (Seiko Instruments Inc., Shizuoka, Japan).

Fabrication of graphene FET devices and transport measurements[33]

A home-built vacuum system with a background pressure of 1.0×10^{-8} mbar was used for the fabrication of the FET devices and transport measurements. A high-purity Au (99.9999%) source was affixed to a tungsten filament in the upper part of the vacuum chamber, and Au atoms were evaporated by direct current resistive heating at a temperature of around 1000 °C. Au films of 500 nm thick were deposited on the graphene–SiO_2/Si surface as the source and drain electrodes, which defined a transport channel of 1 mm in length and 5 mm in width. The FET devices were attached to a ceramic heater with a temperature that could be changed up to 150 °C. Before the FET tests, the devices were *in situ* annealed at 100 °C for 2 h to eliminate possible pre-existing adsorbates (*e.g.* H_2O, O_2 and/or other molecules). During the FET tests, a 1.0 V direct current was applied between the source and drain, while a V_g ranging from −100 to +100 V was applied to the bottom of the SiO_2/Si substrate. The I_{ds} was monitored as a function of V_g through an electrical feed-through.

Acknowledgements

References

1 K. S. Novoselov, A. K. Geim, S. V. Morozov, D. Jiang, Y. Zhang, S. V. Dubonos, I. V. Grigorieva and A. A. Firsov, *Science*, 2004, **306**, 666–669.
2 M. I. Katsnelson, *Mater. Today*, 2006, **10**, 20–27.
3 A. K. Geim and K. S. Novoselov, *Nat. Mater.*, 2007, **6**, 183–191.
4 K. S. Novoselov, A. K. Geim, S. V. Morozov, D. Jiang, M. I. Katsnelson, I. V. Grigorieva, S. V. Dubonos and A. A. Firsov, *Nature*, 2005, **438**, 197–200.

5 Y. Zhang, Y. W. Tan, H. L. Stormer and P. Kim, *Nature*, 2005, **438**, 201–204.

6 X. Huang, Z. Yin, S. Wu, X. Qi, Q. He, Q. Zhang, Q. Yan, F. Boey and H. Zhang, *Small*, 2011, **7**, 1876.

7 X. Du, I. Skachko, A. Barker and E. Y. Andrei, *Nat. Nanotechnol.*, 2008, **3**, 491.

8 B. Standley, W. Bao, H. Zhang, J. Bruck, C. N. Lau and M. Bockrath, *Nano Lett.*, 2008, **8**, 3345.

9 J. S. Bunch, A. M. van der Zande, S. S. Verbridge, I. W. Frank, D. M. Tanenbaum, J. M. Parpia, H. G. Craighead and P. L. McEuen, *Science*, 2007, **315**, 490.

10 J. R. Williams, L. DiCarlo and C. M. Marcus, *Science*, 2007, **317**, 638.

11 X. Li, W. Cai, J. An, S. Kim, J. Nah, D. Yang, R. Piner, A. Velamakanni, I. Jung, E. Tutuc, S. K. Banerjee, L. Colombo and R. S. Ruoff, *Science*, 2009, **324**, 1312–1314.

12 Y. Gong, X. Zhang, G. Liu, L. Wu, X. Geng, M. Long, X. Cao, Y. Guo, W. Li, J. Xu, M. Sun, L. Lu and L. Liu, *Adv. Funct. Mater.*, 2012, **22**, 3153–3159.

13 A. Reina, X. Jia, J. Ho, D. Nezich, H. Son, V. Bulovic, M. S. Dresselhaus and J. Kong, *Nano Lett.*, 2009, **9**, 30–35.

14 T. Ohta, A. Bostwick, T. Seyller, K. Horn and E. Rotenberg, *Science*, 2006, **313**, 951–954.

15 Q. Huang, J. J. Kim, G. Ali and S. O. Cho, *Adv. Mater.*, 2013, **25**, 1144–1148.

16 S. Stankovich, D. A. Dikin, G. H. B. Dommett, K. M. Kohlhaas, E. J. Zimney, E. A. Stach, R. D. Piner, S. T. Nguyen and R. S. Ruoff, *Nature*, 2006, **442**, 282–286.

17 Y. W. Zhu, M. D. Stoller, W. W. Cai, A. Velamakanni, R. D. Piner, D. Chen and R. S. Ruoff, *ACS Nano*, 2010, **4**, 1227–1233.

18 Y. Hao, M. S. B. Bharathi, L. Wang, Y. Liu, H. Chen, S. Nie, Xi. Wang, H. Chou, C. Tan, B. Fallahazad, H. Ramanarayan, C. W. Magnuson, E. Tutuc, B. I. Yakobson, K. F. McCarty, Y. Zhang, P. Kim, J. Hone, L. Colombo and R. S. Ruoff, *Science*, 2013, **342**, 720–723.

19 P. W. Sutter, J.-I. Flege and E. A. Sutter, *Nat. Mater.*, 2008, **7**, 406–411.

20 I. Pletikosić, M. Kralj, P. Pervan, R. Brako, J. Coraux, A. T. N'Diaye, C. Busse and T. Michely, *Phys. Rev. Lett.*, 2009, **102**, 056808.

21 B. Dai, L. Fu, Z. Zou, M. Wang, H. Xu, S. Wang and Z. Liu, *Nat. Commun.*, 2011, **2**, 522–527.

22 Y. Wu, H. Chou, H. Ji, Q. Wu, S. Chen, W. Jiang, Y. Hao, J. Kang, Y. Ren, R. D. Piner and R. S. Ruoff, *ACS Nano*, 2012, **6**, 7731–7738.

23 Y. Zhang, L. Y. Zhang and C. W. Zhou, *J. Am. Chem. Soc.*, 2013, **46**, 2329–2339.

24 Y. Wu, Y. Hao, H. Y. Jeong, Z. Lee, S. Chen, W. Jiang, Q. Wu, R. D. Piner, J. Kang and R. S. Ruoff, *Adv. Mater.*, 2013, **25**, 6744–6751.

25 X. Li, W. Cai, L. Colombo and R. S. Ruoff, *Nano Lett.*, 2009, **9**, 4268–4272.

26 J. D. Wood, S. W. Schmucker, A. S. Lyons, E. Pop and J. W. Lyding, *Nano Lett.*, 2011, **11**, 4547–4554.

27 Q. T. Jiang, M. Nowell, B. Foran, A. Frank, R. H. Havemann, V. Parihar, R. A. Augur and J. D. Luttmer, *J. Electron. Mater.*, 2002, **31**, 10–15.

28 T. H. Ly, D. L. Duong, Q. H. Ta, F. Yao, Q. A. Vu, H. Y. Jeong, S. H. Chae and Y. H. Lee, *Adv. Funct. Mater.*, 2013, **23**, 5183–5189.

29 S. P. Surwade, Z. Li and H. Liu, *J. Phys. Chem. C*, 2012, **116**, 20600–20606.

30 Y. Ren, S. Chen, W. Cai, Y. Zhu, C. Zhu and R. S. Ruoff, *Appl. Phys. Lett.*, 2010, **97**, 053107.

31 X. Li, Y. Zhu, W. Cai, M. Borysiak, B. Han, D. Chen, R. D. Piner, L. Colombo and R. S. Ruoff, *Nano Lett.*, 2009, **9**, 4359.

32 K. T. Chan, J. B. Neaton and M. L. Cohen, *Phys. Rev. B: Condens. Matter*, 2008, **77**, 235430.

33 Y. Wu, W. Jiang, Y. Ren, W. Cai, W. H. Lee, H. Li, R. D. Piner, C. W. Pope, Y. Hao, H. Ji, J. Kang and R. S. Ruoff, *Small*, 2012, **8**, 3129–3136.